Journal of NAMP 73 (2026) 99-112

The Nigerian Association of Mathematical Physics

Journal homepage: https://nampjournals.org.ng

MATHEMATICAL MODEL FOR COVID-19-PNEUMONIA DYNAMICS WITH VACCINATION AND ANTIVIRAL THERAPY.

***OLUWAROTIMI A.O., KOLAWOLE M.K., POPOOLA, A.O.**
Department of Mathematical Sciences, Faculty of Basic and Applied Sciences, Osun State University, Osogbo, Nigeria

ARTICLE INFO

Article history:
Received xxxxx
Revised xxxxx
Accepted xxxxx
Available online xxxxx

Keywords:
Rainfall, Markov chain, Stationary distribution, Mixing time, Total variation distance

ABSTRACT

This study developed a seven-compartment COVID-19-pneumonia model This study develops a seven-compartment COVID-19-pneumonia model to assess the combined effects of pre-variant vaccination and antiviral therapy on transmission and pneumonia progression. The basic reproduction number was derived using the next-generation matrix, while equilibrium, stability, sensitivity, uncertainty, and Laplace-Adomian analyses characterized the dynamics using initial conditions from Osogbo, Nigeria. Vaccination and antiviral therapy jointly reduced infection and pneumonia burden; 60% vaccine protection with 40% antiviral uptake prevented more than 70% of projected pneumonia cases. Transmission, vaccine protection, and antiviral suppression were the dominant parameters. Coordinated deployment can therefore reduce severe disease and support COVID-19 control in resource-constrained settings.

1. Introduction

The emergence of SARS-CoV-2 in December 2019 triggered a global health crisis. COVID-19 presents with variable clinical outcomes ranging from asymptomatic or mild infection to severe viral pneumonia and acute respiratory distress syndrome [1, 2]. Viral pneumonia, driven by viral replication and dysregulated immune responses, remains a key contributor to morbidity and mortality, making it crucial to understand its progression for clinical management and health-system preparedness. SARS-CoV-2 variants differ clinically. Wuhan strains caused marked pulmonary disease [3, 4], Delta increased transmissibility and pneumonia among unvaccinated individuals [5], while Omicron favoured upper-respiratory infection but remained dangerous to older and immunocompromised people [6, 7, 8]. COVID-19 pneumonia results from epithelial injury and excessive inflammation, causing hypoxemia and elevated CRP, ferritin, and D-dimer [9, 10, 11].

*Corresponding author: **OLUWAROTIMI A.O.**
E-mail address: aderonke.oluwarotimi1@ gmail.com,
https://doi.org/10.60787/jnamp.vol73no.731

Severe outcomes are linked to age, comorbidities, high viral load, and delayed care [11, 12]. Vaccination reduces severe disease, although immune-evasive variants weaken protection against infection [8].

Early antivirals may reduce viral load, corticosteroids improve survival, and remdesivir has variable efficacy [13, 14], especially where intensive-care capacity is limited.

SEIR-type models have incorporated variant transmission, pneumonia, hospitalization, and recovery to estimate reproduction numbers and key control parameters [15, 16]. LADM provides rapidly convergent series solutions for nonlinear epidemic models [17, 18]. However, vaccination and antiviral therapy are rarely studied jointly [15, 16].

This study therefore models their separate and combined effects on infection and pneumonia, identifies influential parameters, and determines thresholds for reducing pneumonia and protecting healthcare capacity.

2 Methods

2.1 Model Formulation

The model considers COVID-19 transmission and pneumonia under variant infection, partial vaccination, and antiviral therapy. The population comprises susceptible (S), exposed (E), mildly infected (I_m), variant infected (I_v), pneumonia (P), treated (T), and recovered (R) individuals. Vaccination reduces severe disease [19, 7], while antivirals limit pneumonia progression. Individuals move through infection, progression, treatment, recovery, and death. The antiviral suppression rate ε is therefore best interpreted as an effective, population-averaged parameter that already combines clinical efficacy and treatment coverage/availability, rather than the efficacy of the drug under conditions of universal access; this distinction is particularly relevant in low- and middle-income settings where antiviral supply is constrained (see Section 4)Figure 1 shows the transitions, while Table 1 defines the variables and parameters.The dynamics are governed by:

$$\left.\begin{aligned}
\frac{\mathrm{d}S}{\mathrm{d}t} &= \Lambda - \beta S(I_m + I_v) - \mu S,\\
\frac{\mathrm{d}E}{\mathrm{d}t} &= \beta S(I_m + I_v) - (\sigma + \mu)E,\\
\frac{\mathrm{d}I_m}{\mathrm{d}t} &= \sigma\phi E - (\gamma_1 + \mu + \omega)I_m + \rho\varepsilon I_v,\\
\frac{\mathrm{d}I_v}{\mathrm{d}t} &= \sigma(1-\phi)E - (\gamma_2 + \mu + \rho)I_v,\\
\frac{\mathrm{d}P}{\mathrm{d}t} &= \rho(1-\varepsilon)I_v - (\gamma_3 + \mu + \delta + \eta)P,\\
\frac{\mathrm{d}T}{\mathrm{d}t} &= \omega I_m + \eta P - (\mu + \tau)T,\\
\frac{\mathrm{d}R}{\mathrm{d}t} &= \gamma_1 I_m + \gamma_2 I_v + \gamma_3 P + \tau T - \mu R.
\end{aligned}\right\} \quad (1)$$

subject to the initial conditions

$$S(0) = S_0, \quad E(0) = E_0, \quad I_m(0) = I_{m0}, \quad I_v(0) = I_{v0}, \quad P(0) = P_0, \quad T(0) = T_0, \quad R(0) = R_0.$$

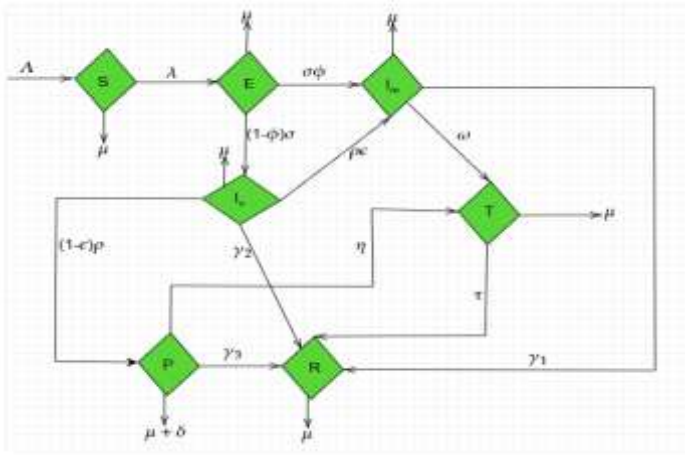

Figure 1: Schematic representation of the model.

Table 1: Model nomenclature and parameter estimates.

Symbol	Description	Value/Estimate	Source
S	Susceptible individuals	201900	[20]
E	Exposed individuals	36	[20]
I_m	Mildly infected individuals	8	[20]
I_v	Variant infected individuals	4	[20]
P	Pneumonia infected individuals	1	[20]
T	Treated (hospitalized) individuals	1	[20]
R	Recovered individuals	156	[20]
Λ	Recruitment rate into the susceptible population	20 persons/day	[20]
β	Transmission rate of infection	$0.38\ \text{day}^{-1}$	[20]
σ	Progression rate from exposed to infected	$0.3571\ \text{day}^{-1}$	[21]
ϕ	Fraction of exposed individuals progressing to mild infection due to pre-variant vaccine protection	0.70	[7]
ε	Antiviral suppression rate (blocks pneumonia progression)	0.66	[22]
ρ	Progression rate from variant infection	0.34	[21]
γ_1	Recovery rate from mild infection	$0.1\ \text{day}^{-1}$	[23]
γ_2	Recovery rate from variant infection	$0.0714\ \text{day}^{-1}$	[23]
γ_3	Recovery rate from pneumonia infection	$0.0476\ \text{day}^{-1}$	[24]
ω	Progression from mild infection to treatment	$0.1\ \text{day}^{-1}$	Assumed
η	Progression from pneumonia to treatment	$0.0476\ \text{day}^{-1}$	[23]
τ	Recovery rate from treatment	$0.0714\ \text{day}^{-1}$	[23]
δ	Disease-induced death rate from pneumonia	0.004	[23]
μ	Natural mortality rate	$0.000025\ \text{day}^{-1}$	[20]

2.1.1. Initial Conditions and Parameter Values

No data fitting or parameter estimation was performed. Initial conditions were based on reported COVID-19 data for Osogbo LGA during the Omicron period, January–March 2022, and literature values. From an estimated population of

$202{,}106$ [20] and 12 daily cases, $S(0) \approx 201{,}900$. Using a three-day incubation period, $E(0) \approx 36$. With $\phi = 0.70$, $I_m(0) \approx 8$ and $I_v(0) \approx 4$. For $\varepsilon = 0.66$ [22], $P(0) = (1-\varepsilon)I_v(0) \approx 1$, while $T(0) \approx 1$. A 14-day infectious period [22] gives $R(0) \approx 156$. Table 1 presents the initial conditions and parameter values.

2.2. Positivity and Boundedness

Theorem 1. For non-negative initial conditions, solutions of system (1) remain non-negative for all $t \geq 0$.

Proof. On each boundary $X_i = 0$, the corresponding derivative is non-negative. Hence, $\mathbb{R}_+^7$ is positively invariant.

Theorem 2. Solutions of system (1) are bounded.

Proof. Let $N = S + E + I_m + I_v + P + T + R.$ Then $\frac{dN}{dt} = \Lambda - \mu N - \delta P \leq \Lambda - \mu N.$ Thus,

$N(t) \leq N(0)e^{-\mu t} + \frac{\Lambda}{\mu}\left(1 - e^{-\mu t}\right),$ and $\limsup_{t\to\infty} N(t) \leq \frac{\Lambda}{\mu}.$ Therefore, the model solutions are bounded.

2.3. Existence and Uniqueness of solution

Theorem 3: For any initial condition $X(0) = X_0 \in \Re_+^{\,7}$, there exists a unique solution X (t) of the initial value problem defined for all t ≥ 0.

Proof: Compute all partial derivatives. For each f_i we list $\partial f_i/\partial x_j$ for $x_j \in \{S, E, I_m, I_v, P, T, R\}$.

For $f_1 = \Lambda - \beta S(I_m + I_v) - \mu S$:

$\left|\frac{\partial f_1}{\partial S}\right| = -\beta(I_m + I_v) - \mu,\ \left|\frac{\partial f_1}{\partial E}\right| = 0,\ \left|\frac{\partial f_1}{\partial I_m}\right| = 0,\ \left|\frac{\partial f_1}{\partial I_v}\right| = 0,\ \left|\frac{\partial f_1}{\partial P}\right| = 0,\ \left|\frac{\partial f_1}{\partial T}\right| = 0,\ \left|\frac{\partial f_1}{\partial R}\right| = 0. \cdots\cdots$

For $f_7 = \gamma_1 I_m + \gamma_2 I_v + \gamma_3 P + \tau T - \mu R$: $\left|\frac{\partial f_7}{\partial S}\right| = 0,\ \left|\frac{\partial f_7}{\partial E}\right| = 0,\ \left|\frac{\partial f_7}{\partial I_m}\right| = \gamma_1,\ \left|\frac{\partial f_7}{\partial I_v}\right| = \gamma_2,\ \left|\frac{\partial f_7}{\partial P}\right| = \gamma_3,\ \left|\frac{\partial f_7}{\partial T}\right| = \tau,\ \left|\frac{\partial f_7}{\partial R}\right| = -\mu$

Each f_i is continuously differentiable in all variables; thus f is C^1, hence locally Lipschitz on $\mathbb{R}^7$. By Picard–Lindelöf, a unique local solution exists for any $X_0 \in \mathbb{R}^7$.

2.4 Equilibrium Points and Basic Reproduction Number

2.4.1 Disease Free Equilibrium

The disease-free equilibrium (DFE) represents the state in which no infection persists in the population. This is achieved by setting all infection related variables to zero: $E = I_m = I_v = P = 0.$ From the equation governing the susceptible class: Therefore, the disease-free equilibrium point is given by:

$$\left(S^0, E^0, I_m{}^0, I_v{}^0, P^0, T^0, R^0\right) = \left(\frac{\Lambda}{\mu}, 0,0,0,0,0,0\right) \tag{2}$$

2.4.2 Endemic Equilibrium

For the system of differential equation in equation (1) the endemic equilibrium is obtained by setting all derivatives to zero and solving for the steady state values with nonzero infection compartments. The Endemic Equilibrium values are:

$$S^* = \frac{\Lambda}{\mu R_0},\quad E^* = \frac{\Lambda(R_0 - 1)}{(\sigma + \mu)R_0},\quad I_v^* = \frac{\sigma\Lambda(R_0 - 1)(1-\phi)}{b(\sigma + \mu)R_0},\quad I_m^* = \frac{\sigma\Lambda(R_0 - 1)}{a(\sigma + \mu)R_0}\left[\phi + \frac{\rho\varepsilon(1-\phi)}{b}\right], P^* = \frac{\rho(1-\varepsilon)\sigma(1-\phi)\Lambda(R_0 - 1)}{bc(\sigma + \mu)R_0},$$

$$T^* = \frac{\Lambda(R_0 - 1)}{(\mu + \tau)(\sigma + \mu)R_0}\left[\frac{\omega\sigma}{a}\left(\phi + \frac{\rho\varepsilon(1-\phi)}{b}\right) + \frac{\eta\rho(1-\varepsilon)\sigma(1-\phi)}{bc}\right], R^* = \frac{\Lambda(R_0 - 1)}{\mu(\sigma + \mu)R_0}\left[\begin{array}{l}\frac{\gamma_1\sigma}{a}\left(\phi + \frac{\rho\varepsilon(1-\phi)}{b}\right) + \frac{\gamma_2\sigma(1-\phi)}{b} + \frac{\gamma_3\rho(1-\varepsilon)\sigma(1-\phi)}{bc} + \\ \frac{\omega\sigma}{a}\left(\phi + \frac{\rho\varepsilon(1-\phi)}{b}\right) + \frac{\eta\rho(1-\varepsilon)\sigma(1-\phi)}{bc}\end{array}\right] \tag{3}$$

This equilibrium point exists provided that the basic reproduction number satisfies $R_0 > 1$.

2.4.3 Basic Reproduction Number

The disease-free equilibrium is $\mathcal{E}_0 = \left(\frac{\Lambda}{\mu}, 0, 0, 0, 0, 0, 0\right)$. Using the infected states $X = (E, I_m, I_v, P, T)^T$, the new-infection and transition matrices at $\mathcal{E}_0$ are

$$F = \begin{pmatrix} 0 & \frac{\beta\Lambda}{\mu} & \frac{\beta\Lambda}{\mu} & 0 & 0 \\ 0 & 0 & 0 & 0 & 0 \\ 0 & 0 & 0 & 0 & 0 \\ 0 & 0 & 0 & 0 & 0 \\ 0 & 0 & 0 & 0 & 0 \end{pmatrix}, \quad V = \begin{pmatrix} a_1 & 0 & 0 & 0 & 0 \\ -\phi\sigma & a_2 & 0 & 0 & 0 \\ -(1-\phi)\sigma & 0 & a_3 & 0 & 0 \\ 0 & 0 & -(1-\varepsilon)\rho & a_4 & 0 \\ 0 & -\omega & 0 & -\eta & a_5 \end{pmatrix}. \tag{4}$$

(Note on notation: in the matrices above, denotes only the diagonal removal-rate coefficient of the pneumonia compartment P in matrix V, and is distinct from the off-diagonal transfer coefficient ρ(1−ε), which represents the rate of inflow into P from Iv.)

Here, $a_1 = \sigma + \mu, \quad a_2 = \gamma_1 + \omega + \mu, \quad a_3 = (1-\varepsilon)\rho + \gamma_2 + \mu,$
$a_4 = \gamma_3 + \eta + \delta + \mu, \quad a_5 = \tau + \mu.$

The basic reproduction number is

$$\mathcal{R}_0 = \rho(FV^{-1}) = \frac{\beta\Lambda\sigma}{\mu a_1}\left(\frac{\phi}{a_2} + \frac{1-\phi}{a_3}\right). \tag{5}$$

Thus, infection declines when $\mathcal{R}_0 < 1$ and persists when $\mathcal{R}_0 > 1$. Each term in Equation (5) admits a clear biological reading: the prefactor $\frac{\beta\Lambda}{\mu(\sigma+\mu)}$ represents new infections generated per unit time at the disease-free equilibrium, discounted by the exposed-class removal rate; the bracketed sum decomposes this into a mild-infection route (weight σφ over its effective removal rate $a_2 = y_1 + \omega + \mu$) and a variant-infection route (weight $\sigma(1-\phi)$ over its effective removal rate $a_3 = y_2 + \rho + \mu$), with the latter further augmented by the factor $\left(1 + \frac{\rho\varepsilon}{a_2}\right)$, reflecting the additional transmission contributed by variant-infected individuals who are subsequently redirected into the mild-infection compartment via antiviral suppression (see Section 2.5).

2.5 Sensitivity analysis of $\mathcal{R}_0$

The normalized sensitivity index $\gamma_p^{\mathcal{R}_0} = \frac{\partial\mathcal{R}_0}{\partial p}\frac{p}{\mathcal{R}_0}$ was used, and the results are presented in Table 2. The reproduction number increases with β, Λ, and σ, but decreases with μ.

The vaccine-protection fraction ϕ has a small negative effect, whereas ε has a positive index because it redirects variant infections to the mild class. Increasing γ_1 or γ_2 shortens infectious periods and reduces $\mathcal{R}_0$.The positive sensitivity of ε follows from $\mathcal{R}_0 = \frac{\beta\Lambda}{\mu a_1}\left[\frac{\sigma\phi}{a_2} + \frac{\sigma(1-\phi)}{a_3}\left(1 + \frac{\rho\varepsilon}{a_2}\right)\right]$, where $a_1 = \sigma + \mu$, $a_2 = \gamma_1 + \omega + \mu$, and $a_3 = \gamma_2 + \rho + \mu$. Thus, $\frac{\partial\mathcal{R}_0}{\partial\varepsilon}\frac{\varepsilon}{\mathcal{R}_0} > 0$ for positive parameter values. At the Table 1 values, the normalized index is 0.16209, agreeing with Table 2. In system (1), the term $\rho\varepsilon I_v$ transfers variant-infected individuals to I_m, while $\rho(1-\varepsilon)I_v$ moves the remainder to P. Since I_m and I_v transmit infection but P does not, increasing ε retains

more individuals in a transmitting class. It may therefore increase $\mathcal{R}_0$ while reducing pneumonia, since $\mathcal{R}_0$ measures transmission rather than severity.

Table 2: **Sensitivity indices of** $\mathcal{R}_0$ parameters

Parameter	Sensitivity Index
Λ	1.000000
β	1.000000
σ	0.000070
μ	-1.000196
ϕ	-0.021911
$\gamma 1$	-0.427705
$\gamma 2$	-0.053204
ρ	-0.091261
ε	0.162090
ω	-0.427705

2.6 Local and Global Stability Analysis

2.6.1 Theorem 4: The disease-free state of the model is Locally Asymptotically Stable if the basic reproduction number $R_0 < 1$ and unstable if $R_0 > 1$.

Proof: The disease-free equilibrium is obtained as the Jacobian matrix of the system of (1) is obtained and evaluated at the disease-free state using the linearization method.

The corresponding Jacobian matrix with respect to system (1) is given by (6)

$$J_{DFE} = \begin{bmatrix} -\mu_1 & 0 & -\beta S^* & -\beta S^* & 0 & 0 & 0 \\ 0 & -(\sigma+\mu) & \beta S^* & \beta S^* & 0 & 0 & 0 \\ 0 & \sigma\phi & -(\gamma_1+\omega+\mu) & \rho\varepsilon & 0 & 0 & 0 \\ 0 & \sigma(1-\phi) & 0 & -(\gamma_2+\rho+\mu) & 0 & 0 & 0 \\ 0 & 0 & 0 & \rho(1-\varepsilon) & -(\gamma_3+\eta+\delta+\mu) & 0 & 0 \\ 0 & 0 & \gamma_1 & \gamma_2 & \gamma_3 & -(\tau+\mu) & 0 \\ 0 & 0 & \omega & 0 & \eta & \tau & -\mu \end{bmatrix} \quad (6)$$

The characteristics polynomial of the Jacobian matrix of Disease Free Equilibrium is given by

Det (J_{DFE} - λI) where **λ** is the **eigen value** and **I** is the **identity matrix**

$$J_{DFE-I\lambda} = \begin{bmatrix} -\mu-\lambda_1 & 0 & -\beta S^* & -\beta S^* & 0 & 0 & 0 \\ 0 & -(\sigma+\mu)-\lambda_7 & \beta S^* & \beta S^* & 0 & 0 & 0 \\ 0 & \sigma\phi & -(\gamma_1+\omega+\mu)-\lambda_6 & \rho\varepsilon & 0 & 0 & 0 \\ 0 & \sigma(1-\phi) & 0 & -(\gamma_2+\rho+\mu)-\lambda_5 & 0 & 0 & 0 \\ 0 & 0 & 0 & \rho(1-\varepsilon) & -(\gamma_3+\eta+\delta+\mu)-\lambda_4 & 0 & 0 \\ 0 & 0 & \gamma_1 & \gamma_2 & \gamma_3 & -(\tau+\mu)-\lambda_2 & 0 \\ 0 & 0 & \omega & 0 & \eta & \tau & -\mu-\lambda_3 \end{bmatrix} \quad (7)$$

Simplifying and solving for the eigen values in (7),we have $\lambda_1 = -\mu$, $\lambda_2 = -(\tau+\mu)$, $\lambda_3 = -\mu$, $\lambda_4 = -(\gamma_3+\eta+\delta+\mu) < 0$. Consequently, the stability of the DFE depends on the remaining 3×3 subsystem$[E, I_m, I_v]$, described by

$$\begin{bmatrix} -(\sigma+\mu)-\lambda_7 & \beta S^* & \beta S^* \\ \sigma\phi & -(\gamma_1+\omega+\mu)-\lambda_6 & \rho\varepsilon \\ \sigma(1-\phi) & 0 & -(\gamma_2+\rho+\mu)-\lambda_5 \end{bmatrix} \quad (8)$$

using Routh-Hurwitz Analysis for Local Stability Consider the 3×3 infected subsystem the characteristic polynomial is $\lambda^3 + a_1\lambda^2 + a_2\lambda + a_3 = 0.$ The coefficients a_1, a_2, and a_3 are given by: $a_1 = (\sigma+\mu)+(\gamma_1+\omega+\mu)+(\gamma_2+\rho+\mu),$
$a_2 = (\sigma+\mu)(\gamma_1+\omega+\mu)+(\sigma+\mu)(\gamma_2+\rho+\mu)+(\gamma_1+\omega+\mu)(\gamma_2+\rho+\mu)-\sigma\phi\beta S^0-\sigma(1-\phi)\beta S^0,$
$a_3 = (\sigma+\mu)(\gamma_1+\omega+\mu)(\gamma_2+\rho+\mu)-(\sigma+\mu)\rho\varepsilon\beta S^0-\sigma\phi(\gamma_2+\rho+\mu)\beta S^0-\sigma(1-\phi)(\gamma_1+\omega+\mu)\beta S^0.$ For our model, the DFE is locally asymptotically stable if all roots of the infected subsystem's characteristic polynomial have negative real parts. Applying the Routh-Hurwitz criterion, this requires $a_1 > 0, \quad a_3 > 0, \quad a_1a_2 > a_3.$

All model parameters are positive, so $a_1 > 0$ is automatically satisfied. The conditions $a_3 > 0$ and $a_1a_2 > a_3$ yield explicit inequalities defining the DFE's stability region.

2.6.2 Uncertainty Quantification

Theorem 2 *Let the uncertain parameter vector be* $\Theta = (\beta,\sigma,\phi,\varepsilon,\rho,\gamma_1,\gamma_2,\gamma_3,\omega,\eta,\tau,\delta).$
Under independent uniform variations $\theta_i \sim U(0.9\theta_i^0, 1.1\theta_i^0),$ a 1000-point Latin-hypercube sample gives the uncertainty intervals and partial rank correlation coefficients (PRCC) reported in Table 2.

Proof. For each sampled vector, the model was solved on $0 \le t \le 10$ days and the outputs
$P_{\max} = \max P(t), \quad P_{10} = P(10), \quad C_P(10) = \int_0^{10} \rho(1-\varepsilon)I_v(t)dt, \; I_{\max} = \max\{I_m(t)+I_v(t)\}$ were calculated. The 95% uncertainty interval was obtained from the 2.5 th and 97.5 th percentiles, while
$\mathrm{CV} = \dfrac{\text{standarddeviation}}{\text{mean}}$. PRCCs were computed from the correlations between the residual parameter ranks and residual output ranks after controlling for the remaining parameters. The results show that ϕ and ε dominate pneumonia uncertainty. The large value of $\mathcal{R}_0$ is produced by the unnormalised incidence $\beta S(I_m + I_v)$ with $\beta = 0.38\text{day}^{-1}$ and is therefore unit-sensitive.

Table 3: Uncertainty propagation and dominant PRCCs.

Output	Baseline	Median	95% interval	CV	Dominant PRCCs
$\mathcal{R}_0$	1.534109×10^6	1.532003×10^6	$[1.351244, 1.738456]\times10^6$	0.0691	β: 0.991, γ_1: –0.947, ω: –0.946
$P_{\max}$	9279.01	9190.04	[6359.88, 12740.98]	0.1809	ϕ: –0.985, ε: –0.977, ρ: 0.565
P_{10}	8918.75	8817.74	[6134.10, 12200.28]	0.1804	ϕ: –0.985, ε: –0.978, η: –0.520
$C_P(10)$	15219.80	15112.93	[10520.03, 20852.22]	0.1805	ϕ: –0.984, ε: –0.976, ρ: 0.560
$I_{\max}$	97153.04	97077.22	[92153.42, 102116.50]	0.0272	σ: 0.987, ω: –0.914, γ_1: –0.911

2.6.3 Global Stability of the Disease-Free Equilibrium

Theorem 5. The disease-free equilibrium $\mathcal{E}_0 = (\Lambda/\mu, 0, 0, 0, 0, 0, 0)$ is globally asymptotically stable in $\Omega = \{X \in \mathbb{R}_+^7 : N \le \Lambda/\mu\}$ if $\mathcal{R}_0 \le 1$, and unstable if $\mathcal{R}_0 > 1$.

Proof. Since $\dot{N} \le \Lambda - \mu N$, then $N(t) \le \Lambda/\mu$ and $S(t) \le S^0 = \Lambda/\mu$ in Ω. Define

$L = E + C_2 I_m + C_3 I_v$, $C_2 = \dfrac{\beta S^0}{a_2}$, $C_3 = \dfrac{\beta S^0 (a_2 + \rho\varepsilon)}{a_2 a_3}$, where $a_2 = \gamma_1 + \omega + \mu$ and $a_3 = \gamma_2 + \rho + \mu$. Along solutions, $\dot{L} \le \beta S^0 (I_m + I_v) - a_1 E + C_2(\sigma\phi E - a_2 I_m + \rho\varepsilon I_v) + C_3[\sigma(1-\phi)E - a_3 I_v]$.

Using $\beta S^0 - C_2 a_2 = 0$ and $\beta S^0 + C_2 \rho\varepsilon - C_3 a_3 = 0$ gives $\dot{L} \le a_1(\mathcal{R}_0 - 1)E \le 0$,

where $\mathcal{R}_0 = \dfrac{\beta S^0}{a_1}\left[\dfrac{\sigma\phi}{a_2} + \dfrac{\sigma(1-\phi)}{a_3}\left(1 + \dfrac{\rho\varepsilon}{a_2}\right)\right]$. The largest invariant set in $\{\dot{L} = 0\}$ satisfies $E = I_m = I_v = P = T = R = 0$ and $S = \Lambda / \mu$. Hence, LaSalle's principle gives convergence to $\mathcal{E}_0$ when $\mathcal{R}_0 \le 1$. For $\mathcal{R}_0 > 1$, local instability follows from Theorem 4. Thus, elimination requires $\mathcal{R}_0 \le 1$; global stability of the endemic equilibrium remains open for future work.

2.7 Model Solution via the Laplace–Adomian Decomposition Method

Because the governing system is a nonlinear autonomous ODE system with no general closed-form solution, LADM was used to obtain a semi-analytical solution. The method applies the Laplace transform to the linear part of each equation, represents the nonlinear force-of-infection term as a series of Adomian polynomials, and recovers each successive solution term by inverse Laplace transformation.

$$\left.\begin{aligned}
L\left[\frac{dS}{dt}\right] &= L[\Lambda - \beta S(I_m + I_v) - \mu S] \\
L\left[\frac{dE}{dt}\right] &= L[\beta S(I_m + I_v) - (\sigma + \mu)E] \\
L\left[\frac{dI_m}{dt}\right] &= L[\sigma\phi E - (\gamma_1 + \mu + \omega)I_m + \rho\varepsilon I_v] \\
L\left[\frac{dI_v}{dt}\right] &= L[\sigma(1-\phi)E - (\gamma_2 + \mu + \rho)I_v] \\
L\left[\frac{dP}{dt}\right] &= L[\rho(1-\varepsilon)I_v - (\gamma_3 + \mu + \delta + \eta)P] \\
L\left[\frac{dT}{dt}\right] &= L[\omega I_m + \eta P - (\tau + \mu)T] \\
L\left[\frac{dR}{dt}\right] &= L[\gamma_1 I_m + \gamma_2 I_v + \gamma_3 P + \tau T - \mu R]
\end{aligned}\right\} \tag{9}$$

Simplifying yields a recurrence relation, which at n=0 yields

$$\left.\begin{aligned}
S_1(t) &= L^{-1}\left(\frac{1}{r}L\left[-\beta\sum_{n=0}^{\infty}Q_0 - \mu\sum_{n=0}^{\infty}S_0\right]\right), \\
E_1(t) &= L^{-1}\left(\frac{1}{r}L\left[\beta\sum_{n=0}^{\infty}Q_0 - (\sigma+\mu)\sum_{n=0}^{\infty}E_0\right]\right), \\
I_{m1}(t) &= L^{-1}\left(\frac{1}{r}L\left[\sigma\phi\sum_{n=0}^{\infty}E_0 - (\gamma_1+\mu+\omega)\sum_{n=0}^{\infty}I_{m0} + \rho\varepsilon\sum_{n=0}^{\infty}I_{v0}\right]\right), \\
.z\, I_{v1}(t) &= L^{-1}\left(\frac{1}{r}L\left[\sigma(1-\phi)\sum_{n=0}^{\infty}E_0 - (\gamma_2+\mu+\rho)\sum_{n=0}^{\infty}I_{v0}\right]\right), \\
P_1(t) &= L^{-1}\left(\frac{1}{r}L\left[\rho(1-\varepsilon)\sum_{n=0}^{\infty}I_{v0} - (\gamma_3+\mu+\delta+\eta)\sum_{n=0}^{\infty}P_0\right]\right), \\
T_1(t) &= L^{-1}\left(\frac{1}{r}L\left[\omega\sum_{n=0}^{\infty}I_{m0} + \eta\sum_{n=0}^{\infty}P_0 - (\tau+\mu)\sum_{n=0}^{\infty}T_0\right]\right), \\
R_1(t) &= L^{-1}\left(\frac{1}{r}L\left[\gamma_1\sum_{n=0}^{\infty}I_{m0} + \gamma_2\sum_{n=0}^{\infty}I_{v0} + \gamma_3\sum_{n=0}^{\infty}P_0 + \tau\sum_{n=0}^{\infty}T_0 - \mu\sum_{n=0}^{\infty}R_0\right]\right).
\end{aligned}\right\} \tag{10}$$

Also the recursive relation at n=1 gives

$$\left.\begin{aligned}
S_2(t) &= L^{-1}\left(\frac{1}{r}L\left[-\beta\sum_{n=0}^{\infty}Q_1-\mu\sum_{n=0}^{\infty}S_1\right]\right),\\
E_2(t) &= L^{-1}\left(\frac{1}{r}L\left[\beta\sum_{n=0}^{\infty}Q_1-(\sigma+\mu)\sum_{n=0}^{\infty}E_1\right]\right),\\
I_{m2}(t) &= L^{-1}\left(\frac{1}{r}L\left[\sigma\phi\sum_{n=0}^{\infty}E_1-(\gamma_1+\mu+\omega)\sum_{n=0}^{\infty}I_{m1}+\rho\varepsilon\sum_{n=0}^{\infty}I_{v1}\right]\right),\\
I_{v2}(t) &= L^{-1}\left(\frac{1}{r}L\left[\sigma(1-\phi)\sum_{n=0}^{\infty}E_1-(\gamma_2+\mu+\rho)\sum_{n=0}^{\infty}I_{v1}\right]\right),\\
P_2(t) &= L^{-1}\left(\frac{1}{r}L\left[\rho(1-\varepsilon)\sum_{n=0}^{\infty}I_{v1}-(\gamma_3+\mu+\delta+\eta)\sum_{n=0}^{\infty}P_1\right]\right),\\
T_2(t) &= L^{-1}\left(\frac{1}{r}L\left[\omega\sum_{n=0}^{\infty}I_{m1}+\eta\sum_{n=0}^{\infty}P_1-(\tau+\mu)\sum_{n=0}^{\infty}T_1\right]\right),\\
R_2(t) &= L^{-1}\left(\frac{1}{r}L\left[\gamma_1\sum_{n=0}^{\infty}I_{m1}+\gamma_2\sum_{n=0}^{\infty}I_{v1}+\gamma_3\sum_{n=0}^{\infty}P_1+\tau\sum_{n=0}^{\infty}T_1-\mu\sum_{n=0}^{\infty}R_1\right]\right).
\end{aligned}\right\} \tag{11}$$

The approximate solution is obtained using the formula

$$\left.\begin{aligned}
&S(t)=\sum_{n=0}^{2}S_n(t), \quad E(t)=\sum_{n=0}^{2}E_n(t), \quad I_m(t)=\sum_{n=0}^{2}I_{mn}(t), \quad I_v(t)=\sum_{n=0}^{2}I_{vn}(t),\\
&P(t)=\sum_{n=0}^{2}P_n(t), \quad T(t)=\sum_{n=0}^{2}T_n(t), \quad R(t)=\sum_{n=0}^{2}R_n(t)
\end{aligned}\right\} \tag{12}$$

The simulations use fifth-order truncated LADM series, which converge rapidly. Equation (12) was evaluated with Table 1 values to obtain practical numerical predictions under real conditions.

$$\left.\begin{aligned}
S(t) &= 201900-3.806069275\times10^5 t+1.921270024\times10^5 t^2-7.184059978\times10^8 t^3\\
&\quad -7.116681157\times10^4 t^4-1.410139905t^5,\\
E(t) &= 36+3.806090235\times10^5 t-2.600847437\times10^5 t^2+7.184369571\times10^8 t^3\\
&\quad +7.116708711\times10^4 t^4+1.410139905t^5,\\
I_m(t) &= 8+8.296320t+4.756983712\times10^4 t^2-2.331790900\times10^4 t^3-0.2336530657t^4,\\
I_v(t) &= 4+2.210980t+2.038686752\times10^4 t^2-1.208351526\times10^4 t^3-0.1519016774t^4,\\
P(t) &= 1+0.363175t+0.1097766243t^2+785.5703288t^3+0.01945562221t^4,\\
T(t) &= 1+1.061775t+0.4731164763t^2+2.070857625\times10^3 t^3+0.05128699483t^4,\\
R(t) &= 156+0.915100t+0.4613534938t^2+1.585673613t^3+0.03927037033t^4.
\end{aligned}\right\} \tag{13}$$

3. Results

3.1. Convergence Analysis

Theorem 1 *Let* $X(t)=\sum_{n=0}^{\infty}X_n(t), \quad X^{[M]}(t)=\sum_{n=0}^{M}X_n(t),$ be the LADM solution and its M th-order truncation. If the model vector field f is Lipschitz continuous on a bounded invariant region Ω with constant L, then the LADM series converges uniformly on $[0,T]$ whenever $q=LT<1$. Moreover, if $\|X_{n+1}\|_\infty \le q\|X_n\|_\infty$, then $\left\|X-X^{[M]}\right\|_\infty \le \frac{q^{M+1}}{1-q}\|X_0\|_\infty$.

Proof. The integral form of the model is $\mathcal{T}X(t)=X(0)+\int_0^t f(X(s))ds.$ For $X,Y\in\Omega$, $\|\mathcal{T}X-\mathcal{T}Y\|_\infty \le LT\|X-Y\|_\infty = q\|X-Y\|_\infty$. Hence, $\mathcal{T}$ is contractive for $q<1$, and the LADM series converges to the unique solution. This follows the convergence arguments used by [27-29].

Let $\mathcal{E}_M(T)=\max_{0\le t\le T}\max_{1\le j\le 7}\frac{|X_j^{[M]}(t)-X_j^{\mathrm{RK45}}(t)|}{1+|X_j^{\mathrm{RK45}}(t)|}$. The decreasing errors in Table 1 establish local convergence since $\mathcal{E}_M<1$.

Table 4: Convergence of the LADM solution on [0,10] days.

Order M	Scaled maximum error $\mathcal{E}_M$
0	1.1629×10^{-7}
2	2.3282×10^{-5}
4	2.0480×10^{-4}
6	9.4082×10^{-3}
8	1.1770×10^{-1}
10	6.0775×10^{-1}

3.2 Numerical Simulation Results

Numerical simulations were conducted to analyze the time-dependent evolution of the model compartments, capture the impact of Omicron progression to pneumonia, and evaluate the effect of antiviral suppression in reducing severe outcomes, using data representative of Osogbo LGA, Nigeria.

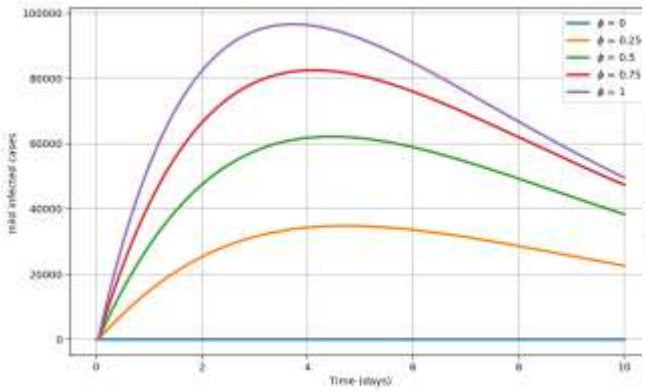

Figure 2: Effect of pre-variant vaccine protection (φ) on the mildly infected population

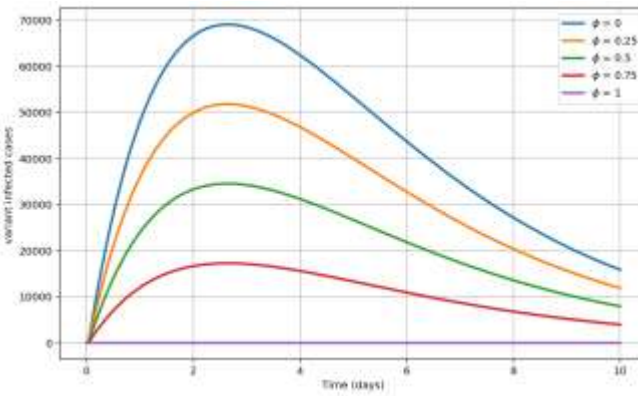

Figure 3: Effect of pre-variant vaccine protection (φ) on the variant infected population

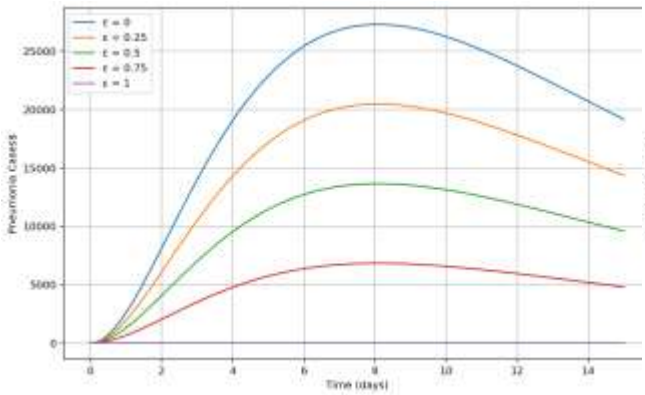

Figure 4: Effect of antiviral suppression rate (ε) on the pneumonia population

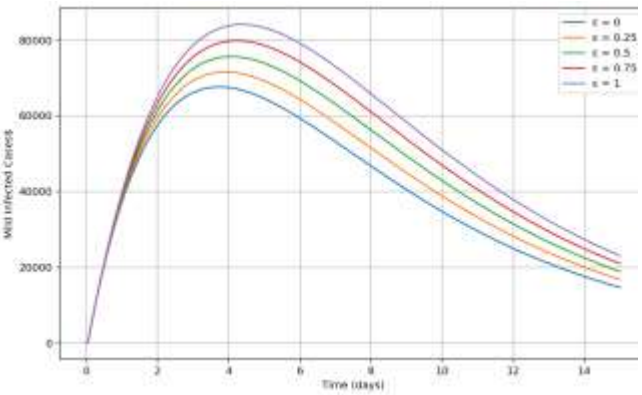

Figure 5: Effect of antiviral suppression rate (ε) on the mildly infected population

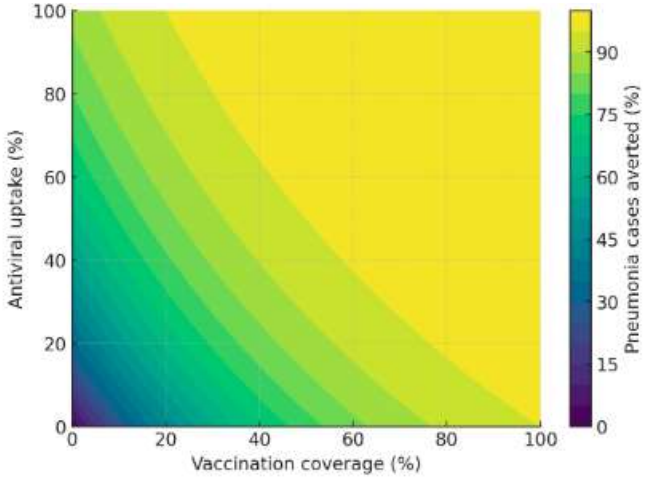

Figure 6: Combined effect of vaccination and antivirals on pneumonia burden

Higher vaccine protection reduced variant infections, while greater antiviral suppression lowered pneumonia and shifted infections toward the milder class (Figures 2-5). The combined intervention produced the largest reduction (Figure 6); about 60% vaccine protection with 40% antiviral uptake prevented more than 70% of projected pneumonia cases

4. Discussion

The model links COVID-19 transmission, pneumonia progression, vaccination, and antiviral therapy. The threshold and stability results show that transmission control depends mainly on β and the durations of mild and variant infection, whereas vaccine protection and antiviral suppression chiefly alter the distribution of clinical outcomes. Vaccination reduced variant infection and antiviral therapy reduced pneumonia, although routing treated variant infections into the mild class can retain some transmission potential. This distinction explains why an intervention may reduce severity without producing an equal reduction in R_0.

Combined coverage performed better than either intervention alone. The practical benefit was greatest when moderate-to-high vaccine protection was accompanied by accessible antiviral treatment, supporting coordinated delivery in settings with limited hospital capacity. LADM produced rapidly convergent approximations and retained explicit parameter dependence, complementing the threshold, sensitivity, and uncertainty analyses.

Future work should extend the model with cost-effectiveness analysis, age-structured dynamics, a formal global stability analysis (which was not established here), and an explicit multi-strain extension in which transmission and severity parameters vary by variant, since the present model is calibrated to a single Omicron-predominant window and does not itself incorporate variant-specific parameter values.

5. Conclusion

This study formulated and analysed a COVID-19-pneumonia model incorporating partial vaccine protection and antiviral therapy. The model established positivity, boundedness, existence, threshold behaviour, and disease-free stability, while sensitivity and uncertainty analyses identified the parameters that most strongly influence transmission and pneumonia burden.

The principal contribution is the joint representation of vaccination and antiviral therapy, which separates effects on transmission from effects on severity. Numerical results show that coordinated intervention substantially lowers pneumonia burden and hospitalization demand.

A combined level of about 60% vaccine protection and 40% antiviral uptake prevented more than 70% of projected pneumonia cases. Control programmes should therefore pair vaccination with timely antiviral access, especially where hospital capacity is limited.

Declaration

The authors declare that there are no competing interests or financial conflicts of interest regarding the publication of this manuscript

References

[1] Zhou X, Chen H, Wang Y, Li Z, Zhao J, Liu Q, (2022). Clinical characteristics of mild COVID-19 cases. J Med Virol. 94(8):3502–3510. doi:10.1002/jmv.27952.

[2] Grasselli, G., Zangrillo, A., Zanella, A., Antonelli, M., Cabrini, L., Castelli, A., Cereda, D., Coluccello, A., Foti, G., Fumagalli, R., Iotti, G., Latronico, N., Lorini, L., Merler, S., Natalini, G., Piatti, A., Ranieri, M. V., Scandroglio, A. M., Storti, E., … Pesenti, A. (2020). Baseline characteristics and outcomes of 1591 patients infected with SARS-CoV-2 admitted to ICUs of the Lombardy region, Italy. JAMA, 323(16), 1574–1581. doi.org/10.1001/jama.2020.5394

[3] Guan, W.J., Ni, Z.-Y., Hu, Y., Liang, W.-H., Ou, C.-Q., He, J.X., Liu, L., Shan, H., Lei, C.-L., Hui, D. S. C., Du, B., Li, L.-J., Zeng, G., Yuen, K.-Y., Chen, R.-C., Tang, C.-L., Wang, T., Chen, P.-Y., Xiang, J., … Zhong, N.-S. (2020). Clinical characteristics of coronavirus disease 2019 in China. New England Journal of Medicine, 382(18), 1708–1720. doi.org/10.1056/NEJMoa2002032

[4] Challen, R., Brooks-Pollock, E., Read, J. M., Dyson, L., Tsaneva-Atanasova, K., & Danon, L. (2021). Risk of mortality in patients infected with SARS-CoV-2 variant of concern 202012/1: matched cohort study. BMI, 372. doi:10.1136/bmj.n579

[5] Yoo, J. W., Kim, W. Y., Chung, C. R., Cho, Y. J., Lee, J., Jegal, Y., ... & Song, J. W. (2024). Early pulmonary fibrosis-like changes between delta and pre-delta periods in patients with severe COVID-19 pneumonia on mechanical ventilation. Scientific reports, 14(1), 26101. doi.org/10.1038/s41598-024-77405-7

6] Ai T, Yang Z, Hou H, Zhan C, Chen C, Lv W (2020). Correlation of Chest CT and RT-PCR Testing for Coronavirus Disease 2019 (COVID-19) in China: A Report of 1014 Cases. Radiology.296(2):E32–E40. doi:10.1148/radiol.2020200642.

[7] Ito, N., Kitahara, Y., Miwata, K., Okimoto, M., & Takafuta, T. (2022). Comparison of COVID-19 pneumonia during the SARS-CoV-2 Omicron wave and the previous non-Omicron wave in a single facility. Respiratory Investigation, 60(6), 772–778. doi.org/10.1016/j.resinv.2022.08.001

[8] Nyberg, T., Ferguson, N. M., Nash, S. G., Webster, H. H., Flaxman, S., Andrews, N., Hinsley, W., Bhatt, S., Cucunubá, Z. M., & Lessler, J. (2022). Comparative analysis of the risks of hospitalisation and death associated with SARS-CoV-2 Omicron (B.1.1.529) and Delta (B.1.617.2) variants in England: A cohort study. The Lancet, 399(10332), 1303–1312. doi.org/10.1016/S0140-6736(22)00462-7

[9] Mehta P, McAuley DF, Brown M, Sanchez E, Tattersall RS, Manson J.J (2020). COVID-19: Consider cytokine storm syndromes and immunosuppression. Lancet;395(10229):1033–1034. doi:10.1016/S0140-6736(20)30628-0.

[10] Wiersinga, W. J., Rhodes, A., Cheng, A. C., Peacock, S. J., & Prescott, H. C. (2020). Pathophysiology, transmission, diagnosis, and treatment of coronavirus disease 2019 (COVID-19): A review. JAMA, 324(8), 782–793. doi.org/10.1001/jama.2020.12839

[11] Zhou, F., Yu, T., Du, R., Fan, G., Liu, Y., Liu, Z., Xiang, J., Wang, Y., Song, B., Gu, X., Guan, L., Wei, Y., Li, H., Wu, X., Xu, J., Tu, S., Zhang, Y., Chen, H., & Cao, B. (2020). Clinical course and risk factors for mortality of adult inpatients with COVID-19 in Wuhan, China: A retrospective cohort study. The Lancet, 395(10229), 1054–1062. doi.org/10.1016/S0140-6736(20)30566-3

[12] Torres A, Cilloniz C, Niederman MS, Menéndez R, Chalmers JD, Wunderink RG (2021), van der Poll T. Pneumonia. Nat Rev Dis Primers. Apr 8;7(1):25. doi: 10.1038/s41572-021-00259-0. PMID: 33833230

[13] Beigel, J. H., Tomashek, K. M., Dodd, L. E., Mehta, A. K., Zingman, B. S., Kalil, A. C., Hohmann, E., Chu, H. Y., Luetkemeyer, A., Kline, S., Lopez de Castilla, D., Finberg, R. W., Dierberg, K., Tapson, V., Ssenator, L., McGettigan, T. H., Bhimraj, A., Coli, K. M., & Lane, H. C. (2020). Remdesivir for the treatment of COVID-19 final report. New England Journal of Medicine, 383(19), 1813–1826. doi.org/10.1056/NEJMoa2007764 [14] Ko, Y., Lee, J., Kim, Y., Kwon, D., & Jung, E. (2021). COVID-19 vaccine priority strategy using a heterogeneous transmission model based on maximum likelihood estimation in the Republic of Korea. International Journal of Environmental Research and Public Health, 18(12), Article 6469. doi.org/10.3390/ijerph18126469

[15] Liossi, S., Tsiambas, E., Maipas, S., Papageorgiou, E., Lazaris, A., & Kavantzas, N. (2023). Mathematical modeling for Delta and Omicron variant of SARS-CoV-2 transmission dynamics in Greece. Infectious Disease Modelling, 8(3), 794–805.

[16] Oh, J., Apio, C., & Park, T. (2022). Mathematical modelling of the impact of Omicron variant on the COVID-19 situation in South Korea. Genomics & Informatics, 20(2), Article e22. doi.org/10.5808/gi.22025

[17] Jeeva, N., Dharmalingam, K. M., Fadugba, S. E., Kekana, M. C., & Adeniji, A. A. (2024). Implementation of Laplace Adomian decomposition and differential transform methods for Sars-Cov-2 model. Journal of applied mathematics & informatics, 42(4), 945-968..doi.org/10.14317/jami.2024.945

[18] Van den Driessche, P., & Watmough, J. (2002). Reproduction numbers and sub-threshold endemic equilibria for compartmental models of disease transmission. Mathematical Biosciences, 180(1–2), 29–48. doi.org/10.1016/S0025-5564(02)00108-6

[19] Bernal, L. J., Andrews, N., Gower, C., Robertson, C., Stowe, J., Tessier, E., Simmons, R., Cottrell, S., Roberts, R., O'Doherty, M., Brown, K., Cameron, C., Stockton, D., McMenamin, J., & Ramsay, M. (2021). Effectiveness of COVID-19 vaccines against the B.1.617.2 (Delta) variant. New England Journal of Medicine, 385(7), 585–594. doi.org/10.1056/NEJMoa2108891

[20] National Bureau of Statistics (NBS). Population and demographic data reports. Abuja (Nigeria): NBS; 2022. [last visited August 15, 2025]. Available from: https://www.nigerianstat.gov.ng/elibrary/read/1241422.

[21] Cai, M., Em Karniadakis, G., & Li, C. (2022). Fractional SEIR model and data-driven predictions of COVID-19 dynamics of Omicron variant. Chaos: An Interdisciplinary Journal of Nonlinear Science, 32(7). doi.org/10.1063/5.0099450

[22] Zhang, H., Ge, C., Fisher, D., Nguyen, H., Musabaev, E., Pronyuk, K., Zhao, L., & Xu, L. (2025). Antiviral treatment for viral pneumonia: Current drugs and natural compounds. Virology Journal, 22(1), 1–10. doi.org/10.1186/s12985-025-02666-1

[23] World Health Organization (WHO). Clinical management of COVID-19: Living guidance. Geneva (Switzerland): WHO; (2022). [last visited August 15, 2025]. Available from: https://www.who.int/publications/i/item/WHO-2019-nCoV-clinical-2022.

[24] Yatera K, Yamasaki K, (2025). Management of the diagnosis and treatment of pneumonia in an aging society. Internal Medicine.64(4):503–517

[25]Zhao L, Wang T, Li J, Xu F, Chen Y, Huang X, et al.(2025) Clinical effectiveness of oral antiviral treatment for non-severe COVID-19 pneumonia. Pneumonia.17:168. doi:10.1186/s41479-025-00168-w.

[26] Nigeria Centre for Disease Control (NCDC). (2025, April 5). Weekly epidemiological report, March 2025 (Vol. 15, No. 12). https://ncdc.gov.ng/reports/weekly

[27] A. I. Alaje and M. O. Olayiwola, "A fractional-order mathematical model for examining the spatiotemporal spread of COVID-19 in the presence of vaccine distribution," Healthcare Analytics, vol. 4, Article 100230, 2023.

[28] M. O. Olayiwola, A. I. Alaje, A. Y. Olarewaju, and K. A. Adedokun, "A Caputo fractional order epidemic model for evaluating the effectiveness of high-risk quarantine and vaccination strategies on the spread of COVID-19," Healthcare Analytics, vol. 3, Article 100179, 2023.

[29] T. A. Ayoola, A. O. Popoola, M. O. Olayiwola, and A. I. Alaje, "Mathematical modeling of chickenpox transmission using the Laplace–Adomian decomposition method," Results in Control and Optimization, vol. 15, Article 100436, 2024.